



A new method to evaluate the brittleness for brittle rock using crack initiation stress level from uniaxial stress–strain curves

Y. Wang¹ · C. H. Li¹ · Y. Z. Hu² · X. L. Zhou¹

Received: 15 July 2017 / Accepted: 6 November 2017 / Published online: 27 November 2017
© Springer-Verlag GmbH Germany, part of Springer Nature 2017

Abstract

Brittleness has been a prevalent descriptor in rock mass engineering and formation fracturing stimulation. Here a new definition of mechanical brittleness index as crack initiation stress level (σ_{ci}/σ_c) is proposed and verified with diorite, granite, marble, sandstone, and shale samples using uniaxial compressive strength (UCS) test. Regression analysis reveals obvious correlation between σ_{ci}/σ_c and four brittleness definitions based on UCS and Brazilian tensile strength (BTS) ($B19 = \sigma_c/\sigma_t$, $B20 = (\sigma_c - \sigma_t)/(\sigma_c + \sigma_t)$, $B21 = (\sigma_c \times \sigma_t)/2$, $B22 = (B21)^{1/2}$). For diorite, granite, marble, and sandstone, significant relationships exist between B19, B20, and B23; however, for anisotropic shale, obvious relationships were found between B21, B22, and B23. It is suggested that σ_{ci}/σ_c can well reflect the heterogeneity and anisotropy of rock and the correlation between B19, B20, B21, B22, and σ_{ci}/σ_c depends on the rock structural fabric. In addition, rock with high brittleness generally has a lower σ_{ci}/σ_c value and fracture easily occurs during sample deformation. It is not the case that formation with higher brittleness is considered as good fracturing candidates. Fracture pattern was obtained for shale samples from X-ray CT scanning, and the results reveal that fracture density is the maximum for sample with the lowest σ_{ci}/σ_c value. The most striking finding is that there exists a good correlation between the stimulated fracture density and σ_{ci}/σ_c , and it implies that a good formation for hydraulic fracturing is not of high brittleness. The proposed brittleness index would be helpful to evaluate the formation fracability and screen hydraulic fracturing candidates.

Keywords Brittleness index · Crack initiation stress · Uniaxial compressive test · Hydraulic fracturing

Introduction

Brittleness of rock is closely related not only to the stability of rock mass engineering, but also to the reservoir stimulation in oil and gas engineering and geothermal

development. Many rock mechanical issues are closely related to rock brittleness, such as rock mass drillability (Protodyakonov 1963; Aubertin 2010; Yarali and Kahraman 2011), rock cutting sawability (Gunaydin et al. 2004; Altindag and Guney 2010), brittle rupture (Hajj-abdolmajida et al. 2003; Cai 2010), rockburst prediction (Feng and Xie 2000), stability of underground structure (Cai et al. 2004), and oil and gas development (Jin et al. 2014; Wang et al. 2014; Zhang et al. 2017). A brittle rock presents some special properties, such as (1) low elongation when acted on loading, (2) fracture failure occurs at small strain, (3) ratio of compressive strength to tensile strength is high, (4) higher resilience, (5) higher percentage of brittle minerals like quartz and minimal proportion of clay minerals, (6) greater internal friction angles, (7) lower Poisson's ratio and higher elastic modulus values, (8) exhibiting intensive failure process, fracture fully developed when fracturing occurs and rocks reach failure suddenly in an intensive way.

So far, various definitions to describe rock brittleness have been proposed by many scholars and many different

✉ Y. Wang
wyzhou@ustb.edu.cn

C. H. Li
lch_ustb@126.com

Y. Z. Hu
huyz@mail.iggcas.ac.cn

X. L. Zhou
zxl_ustb@126.com

¹ Beijing Key Laboratory of Urban Underground Space Engineering, Department of Civil Engineering, School of Civil and Resource Engineering, University of Science and Technology Beijing, Beijing 100083, China

² Key Laboratory of Shale Gas and Geoengineering, Institute of Geology and Geophysics, Chinese Academy of Sciences, Beijing 100029, China

influential factors have been taken into consideration, including rock mechanical parameter, mineral composition, rock hardness. Each definition has its applicability and reliability for the specific required purpose. In shale gas development field, reasonable definition of brittleness is important to shale gas recovery. Hydraulic fracturing technique has been viewed as a widely used way to gain enormous amount of gas resource (Jin et al. 2014; Zhang et al. 2017). During hydraulic fracturing treatment, hydraulic fractures interact with preexisting natural fractures and complex fracture network forms. The low pore and low permeability characteristics of shale reservoirs can be improved when formation of complex fracturing network occurs. However, many factors affect the formation of an effective fracture network, among which the formation brittleness plays a predominant role. Currently, many scholars have used brittleness to evaluate the fracability of reservoirs. Generally speaking, it has been considered that good fracturing formations should have higher brittleness (Wang and Gale 2009; Wang et al. 2016; Li et al. 2012; Chong et al. 2010; Zhang et al. 2017). However, this point is not always true, because a phenomenon of fracture barrier may occur for higher brittleness formations (Bruner and Smosna 2011; Jin et al. 2014); this is adverse to form complex fracturing network during fracturing treatment. The current brittleness definition approaches cannot reflect the formation fracability; therefore, we should seek new brittleness definition method or take into account other parameters to evaluate the fracability of formations.

In this work, plenty of UCS tests have been done for various kinds of rock to seek a new brittleness definition, which is named as crack initiation stress level (σ_{ci}/σ_c). Based on the raw experimental data, because of the close relationship between the rock brittleness and its mechanical properties, we try to explore the relations between brittleness index defined using uniaxial compressive strength, σ_c , and tensile strength, σ_t . Our research is mainly focused on the relationship between B19, B20, B21, B22 (brittleness index based on strength ratio), and σ_{ci}/σ_c . To the author's knowledge, so far no experimental results have been published that describe the link between brittleness index and σ_{ci}/σ_c . The aim of this study is to seek a new brittleness definition to well reflect the fracture density after UCS test. To begin with, the methods to define rock brittleness index have been summarized from the published literature. Then, the link between B19, B20, B21, B22, and σ_{ci}/σ_c was investigated using theoretical and experimental investigation. Finally, the reliability of σ_{ci}/σ_c to reflect fracture pattern has been deeply discussed. From our results, only by uniaxial compression test can the brittleness index be established easily and quickly, and also it

can be used as a preliminary index in reservoir brittleness evaluation.

Methods

Quantification of brittleness

Brittleness is one of the comprehensive properties of rock material. It is influenced by many internal and external factors. The internal factors refer to the heterogeneity of rock, including mineral particles, texture, and structure; the external factors are the non-uniform stress loading on rock under certain stress conditions, which leads to local damage and then forms multidimensional failure surfaces. After literature review, methods for determining the brittleness index are based on six approaches. These methods include (1) uniaxial compressive strength and Brazilian tensile strength, (2) stress–strain curve methods, (3) hardness test, or impact test, (4) porosity and grain size, (5) mineral composition, and (6) geophysical method. The detailed methods of brittleness definitions are summarized in Table 1. The proportion of these methods to determine brittleness is about 35.32, 42.98, 6.9, 1.4, 11.1, and 2.3%, respectively. It can be concluded that the mechanical properties hold the biggest percentage which is closely related to brittleness.

Method for determining crack initiation stress

Many methods have been proposed to obtain the crack initiation stress, σ_{ci} , for brittle rock, and these methods mainly include (1) volumetric strain or crack volumetric strain methods, (2) lateral strain methods, and (3) acoustic emission method. These methods were summarized in detail by Nicksiar and Martin (2012), and a new method called the LSR (lateral strain response method) was also proposed through lots of laboratory test. In this work, the calculation of σ_{ci} used the crack volumetric strain method. As for brittle rock samples, in both uniaxial and triaxial experiments, brittle rocks experienced four typical stages: (1) crack closure stage, in the axial strain curve, it presents as the starting point of linearity; (2) crack initiation and stable crack propagation, an inflection point in the lateral strain occurs during sample deformation; (3) start of unstable crack propagation, this corresponds to the maximum volumetric strain in the volumetric strain curve; and (4) peak stage, it occurs after failure of sample and after the peak stress in the axial strain. Many researchers have proved that when a stress value exceeds the crack initiation during stress–strain responses, crack initiates and propagates (Martin and Chandler 1994; Bieniawski 1967; Brace et al. 1966; Diederichs et al. 2004). Figure 1 plots the complete stress strain curve and the

Table 1 Summary of current brittleness index definitions and testing methods

Reference	Formula	Variable declaration	Test method
Honda and Sanada (1956)	$B1 = (H_m - H)/K$	H is macro-hardness; H_m is micro-hardness; K is bulk modulus	Hardness test
Protodyakonov (1963)	$B2 = q/\sigma_c$	q is weight percentage of debris (< 0.6 mm diameter); σ_c is uniaxial compressive strength	Proto impact test
Yagiz (2002)	$B3 = F_{max}/P$	F_{max} is the maximum impact load; P is the maximum impact depth	Proto impact test
Bishop (1967)	$B4 = (\tau_p - \tau_r)/\tau_p$	τ_p is peak shear strength; τ_r is residual shear strength	Stress-strain test
Vahid and Peter (2003)	$B5 = (\epsilon_p - \epsilon_r)/\epsilon_p$	ϵ_p is peak of strain, ϵ_r is residual strain	Stress-strain test
Aubertin (2010)	$B6 = A_2/A_1$	A_1, A_2 are areas of stress strain, the slope corresponds to 50% peak strength, which divides the curve into two parts	Stress-strain test
Hucka and Das (1974)	$B7 = \epsilon_f/\epsilon$	ϵ_f and ϵ are recoverable and total strains	Stress-strain test
Hucka and Das (1974)	$B8 = W_f/W$	W_r and W_t are recoverable and total strain energies	Stress-strain test
Feng and Xie (2000)	$B9 = \alpha\sigma_c\epsilon_f/\sigma_f\epsilon_b$	σ_c and σ_f are compressive and tensile strengths, ϵ_f and ϵ_b are pre-peak and post-peak strains; α is accommodation coefficient and it is generally 0.1	Stress-strain test
Rickman et al. (2008)	$B10 = (\bar{E} + \bar{\nu})$	\bar{E} and $\bar{\nu}$ are normalized elastic modulus and Poisson's ratio	Stress-strain test
Yagiz and Gokceoglu (2010)	$B11 = 0.198\sigma_c - 2.174\sigma_t + 0.913\rho - 3.807$	σ_c and σ_t are unconfined compressive strength and tensile strength, respectively; ρ is the density	Stress-strain test
Modified from Rickman et al. (2008)	$B12 = (E_n + \nu_n)/2$	E_n and ν_n are normalized dynamic Young's modulus and dynamic Poisson's ratio	Stress-strain test
Tarasov (2001)	$B13 = dW_f/dW_c = (E - M)/M$	W_r and W_e are fracture energies after and before failure	Stress-strain test
Li et al. (2012)	$B14 = (\epsilon_{BRIT} - \epsilon_n)/(\epsilon_m - \epsilon_n) + \alpha CS_{BRIT} + \beta C_{S_{BRIT}} + \eta$	ϵ_{BRIT} is peak strain parameter, ϵ_m and ϵ_n are the maximum and minimum strain values; CSBRIT is shape parameter for post-peak stress strain curve; α, β, η are standardized coefficients	Stress-strain test
Xia et al. (2017)	$B15 = \frac{\sigma_p - \sigma_r}{\epsilon_r - \epsilon_p} + \frac{(\sigma_p - \sigma_r)(\epsilon_r - \epsilon_p)}{\sigma_p \epsilon_p}$	ϵ_p and ϵ_r are peak strain and residual strain; σ_p and σ_r are peak strength and residual strength	Stress-strain test
Hajjabdolmajid (2003)	$B16 = (\epsilon_f^p - \epsilon_c^p)/\epsilon_c^p$	ϵ_f^p and ϵ_c^p are the plastic strains when the cohesive strength reduces to the residual value and the friction strength is fully mobilized	Stress-strain test-CWF model
Tarasov and Potvin (2013)	$B17 = M - E/M$	E and M are unloading elastic modulus and post-peak elastic modulus	UCS test
Wang et al. (2015)	$B18 = \frac{1}{\ln\left(\frac{E_{luc}}{\sigma_{ucs}}\right)}$	E_{luc} and σ_{ucs} are peak axial strain and peak axial stress	UCS test

Table 1 (continued)

Reference	Formula	Variable declaration	Test method
Hucka and Das (1974)	$B19 = \sigma_c / \sigma_t$	σ_c and σ_t are compressive strength and tensile strength	UCS test and Brazilian test
Hucka and Das (1974)	$B20 = (\sigma_c - \sigma_t) / (\sigma_c + \sigma_t)$	σ_{ci} and σ_c are the crack initiation stress and unconfined compressive strength	
Hucka and Das (1974)	$B21 = \sigma_c \cdot \sigma_t / 2$	E is elastic modulus; ν is Poisson's ratio	
Altindag (2002)	$B22 = (\sigma_c \cdot \sigma_t / 2)^{1/2}$	E is elastic modulus; ρ is the density; ν is Poisson's ratio	
Defined in this paper	$B23 = \sigma_{ci} / \sigma_c$	Φ is the frictional angle	Mohr circle or logging data
Luan et al. (2014)	$B24 = E / \nu$	H is the hardness coefficient; KIC is fracture toughness	Hardness and fracture toughness test
Sun et al. (2013)	$B25 = E_p / \nu$	G_F , E , and σ_t are fracture energy, elastic modulus, and tensile strength; L is Hilleborg length	Stress-strain test and fracture toughness test
Altindag (2002)	$B26 = \sin(\phi)$	K_{IC} is fracture toughness; σ_y is yield stress; h is characteristic length of the tested sample	Fracture toughness test
Hucka and Das (1974)	$B27 = 45^\circ + \phi / 2$	ϵ_{ij} is the unrecoverable axial strain. $\epsilon_{ij} < 3\%$ brittleness; $3\text{--}5\%$ brittle-plasticity; $> 5\%$ plasticity	Stress-strain test
Lawn and Marshall (1979)	$B28 = H / K_{IC}$	U_c is the elastic energy at the peak stress; U_{total} is the total fracture energy, which is composed of pre-peak energy and post-peak energy	Stress-strain test
Bazant and Kazemi (1990)	$B29 = L \sigma_t^2 / E G_F$	U_c is the elastic energy at the peak stress; U_{post} is the post-peak energy	Stress-strain test
Bazant and Kazemi (1990)	$B30 = E G_F / \sigma_t^2$	U_{peak} is the pre-peak energy; U_{total} is the total fracture energy, which is composed of pre-peak energy and post-peak energy	Stress-strain test
Bazant and Kazemi (1990)	$B31 = K_{IC} / (\sigma_y h^{0.5})$	H is hardness; K_{IC} is fracture toughness; and E is Young's modulus	Hardness, stress-strain, and fracture toughness test
Andreev (1995)	$B32 = \epsilon_{ij} \cdot 100\%$	Weight ratio for fragment with its diameter less than 11.2 mm	Impact test
Munoz et al. (2016a)	$B33 = U_d / U_{total}$	P_{inc} and P_{dec} are average increment and decrement of forces	Punch penetration test
Munoz et al. (2016b)	$B34 = U_d / U_{post}$	c is crack length, d is indent size for Vickers indents at a specified load, empirically related to H/KIC	Indentation test
Munoz et al. (2016b)	$B35 = U_{peak} / U_{total}$	W_{dol} and W_{qtz} are weights of dolomite and quartz; W_{Tot} is total mineral weight	Mineralogical logging or XRD
Quinn and Quinn (1997)	$B36 = H/E/K^2$		
Blindheim and Bruland (1998)	$B37 = S_{20}$		
Copur et al. (2003)	$B38 = P_{inc} / P_{dec}$		
Sehgal et al. (1995)	$B39 = c/d$		
Wang and Gate (2009)	$B40 = (W_{qtz} + W_{dol}) / W_{total}$		

Table 1 (continued)

Reference	Formula	Variable declaration	Test method
Jarvie et al. (2007a, b)	$B41 = W_{qtz}/W_{total}$	W_{qtz} and W_{Tot} are weight of quartz and total mineral weight	
Jin et al. (2014)	$B42 = (W_{QFM} + W_{Carb})/W_{Tot}$	W_{QFM} is weight of feldspar, quartz, and mica; W_{Carb} is weight of carbonate minerals consisting of dolomite, calcite, and other carbonate components. W_{Tot} is total mineral weight	
Rickman (2008)	$B43 = (W_{qtz} + W_{crab})/W_{total} = (W_{QFM} + W_{calcite} + W_{dolomite})/W_{Tot}$	W_{Tot} is total mineral weight. W_{QFM} is weight of feldspar, quartz, and mica; W_{Carb} is weight of carbonate minerals consisting of calcite, dolomite, and other carbonate components	Laboratory test or well log data
Jin et al. (2014a, b)	$B44 = -1.8748 \times \varphi + 0.9679$	φ is the porosity; θ is the internal friction angle	
Nygård (2006)	$B45 = OCR^b = \left(\frac{\sigma'_v \max}{\sigma'_v}\right)^b$	OCR: over-consolidation ratio; b is an empirical constant; σ'_v is the current effective vertical stress; $\sigma'_{v,ind}$ is the maximum effective vertical stress	
Guo et al. (2012)	$B46 = \lambda/(\lambda + 2\mu)$	λ is Lamé's first parameter; μ is shear modulus	
Chen et al. (2014)	$B47 = E/\lambda$	E is Young's modulus	

crack volumetric stress strain curves for brittle rock. The crack initiation stress, σ_{ci} , can be determined using the curves.

Research idea

From Table 1, most of the brittleness definitions are based on rock mechanical parameters. Among many of those parameters, the two basic rock mechanics properties of σ_c and σ_t can be easily obtained by simple laboratory testing; they are the two important and fundamental parameters in rock mechanics. Using those two basic rock mechanical parameters, the following four definitions are based on this understanding (as shown in Table 1):

$$B19 = \sigma_c/\sigma_t; \tag{1}$$

$$B20 = (\sigma_c - \sigma_t)/(\sigma_c + \sigma_t); \tag{2}$$

$$B21 = \sigma_c \cdot \sigma_t/2; \tag{3}$$

$$B22 = (\sigma_c \cdot \sigma_t/2)^{1/2}. \tag{4}$$

Crack initiation stress is also viewed as an important rock mechanical parameter; it is associated with the type of rock, mineral content, and the defects that preexist in the rock, such as micro-cracks, grain boundaries, and lattice defects. The first crack initiation criterion for brittle material was proposed by Griffith. Crack starts to initiate when $K_I = K_{IC}$, where K_{IC} is named as the fracture toughness of the rock and its value can be calculated from the rock's tensile strength in the form of $\sigma_t = 6.88K_{IC}$ (Sih 1974). Zhang et al. (2016) have proved that $\sigma_c = (55-82) K_{IC}$ and $\sigma_c/\sigma_t = 8-12$. Cai et al. (2004) studied the relationship between crack initiation stress and strength ratio, when the half crack length equals 0.5, 1, and 1.5 mm, respectively. In the aspect of mechanical property, σ_{ci}/σ_c can be functioned as the fracture toughness, tensile strength, and compressive strength. From the analysis above, σ_{ci}/σ_c is also close related to the tensile strength and compressive strength. It can be assumed that σ_{ci}/σ_c may be expressed as a function of fracture toughness:

$$\left. \begin{matrix} \sigma_{ci} = f(\sigma_c, \sigma_t) \\ \sigma_c = f(K_{IC}) \\ \sigma_t = f(K_{IC}) \end{matrix} \right\} \Rightarrow \sigma_{ci}/\sigma_c = f(K_{IC}). \tag{5}$$

As stated above, fracture toughness and σ_c and σ_t are closely related. Combined with σ_{ci}/σ_c and these strength parameters, we assume that there may be a certain relationship between the brittleness index and σ_{ci}/σ_c , and the relation can be expressed as:

$$\left. \begin{matrix} B = f(\sigma_c, \sigma_t) \\ K_{IC} = f(\sigma_c, \sigma_t) \end{matrix} \right\} \Rightarrow B = f(\sigma_{ci}/\sigma_c). \tag{6}$$

In uniaxial compression tests, σ_{ci} and σ_c are not equal. We can use the ratio of these two indices to reflect the difference under a compression test. For brittle rock, generally, σ_c is not used alone to reflect the brittleness of rock, because a rock which is much more brittle may have low σ_c , vice versa. To reasonably reflect the brittleness, in Table 1, we summarize the brittleness definitions using σ_c and σ_t . In addition, to deeply study the issue of crack initiation in brittle rock, Cai (2010) has done plenty of theoretical and experimental analyses and found that there exists a certain relation between tensile strength and crack initiation stress. Therefore, in this work, the mechanical parameters of σ_c and σ_{ci} are used to redefine the brittleness, as below:

$$B23 = \sigma_{ci} / \sigma_c. \quad (7)$$

B23 reflects the difference in heterogeneity and texture. For rock with fine structured particle, this value is generally larger than rock with medium and coarse particles (Cai 2010). In the next section, a series of experimental works have been done for different rocks to investigate the relationship between brittleness B23 and B19, B20, and B21.

Testing and test results

Tested materials

The rock samples used in this work include diorite, granite, marble, sandstone, and shale. The gray diorite was obtained from the Hot ha tal hydropower station in Xinjiang, China. It is a kind of medium- to coarse-grained rock, with an average particle size between 2 and 4 mm. The granite is obtained from 500 to 600 m depth in Alxa area of China, it is a kind of extreme heterogeneous and coarse-grained rock, and the color of the rock is pink, with its density of 2.67 g/cm^3 . Plenty of brittle minerals exist in the granite sample, such as *k*-feldspar with grain size of 2.0–20 mm is 30%, plagioclase with grain size of 2.0–6.0 mm is about 35%, and quartz with grain size of 2.0–3.0 mm is about 35%. The white marble is obtained from a stone pit, with a density of 2.51 g/cm^3 . The sandstone was obtained from a tight gas sandstone reservoir; it is a kind of fine-grained red brown stone, obtained from Tarim Basin, China; and the density of the sample is about 2.58 g/cm^3 . The shale was from Longmaxi Formation in the Lower Silurian located in Shizhu County, Chongqing,

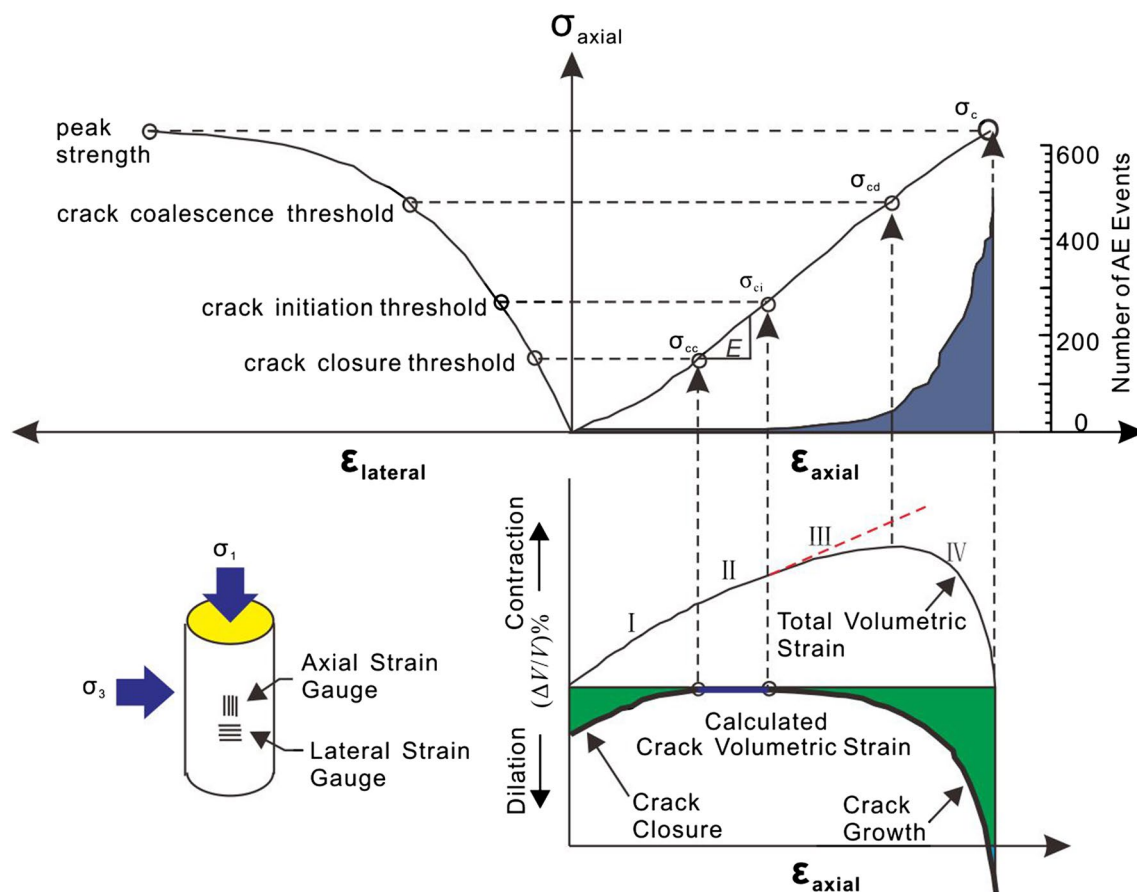


Fig. 1 Crack evolution process in the stress–strain diagram (modified after Martin and Chandler 1994). Note that the axial and lateral strains are measured using experiment, and the crack volumetric strain and volumetric strain curve are calculated

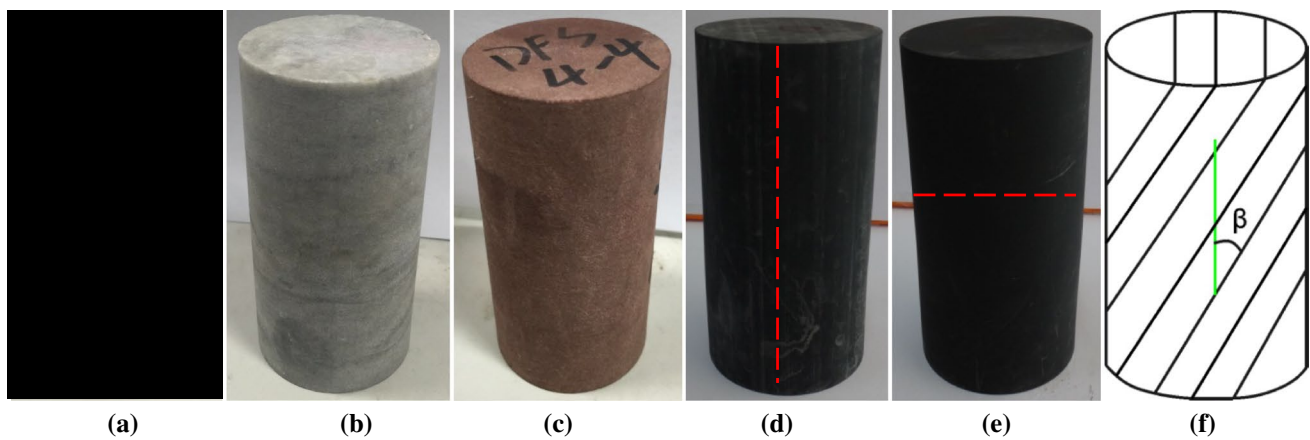


Fig. 2 Partial tested rock samples in this work. a Granite. b Marble. c Sandstone. d Shale, $\beta = 0^\circ$. e Shale, $\beta = 90^\circ$. f Shale orientation

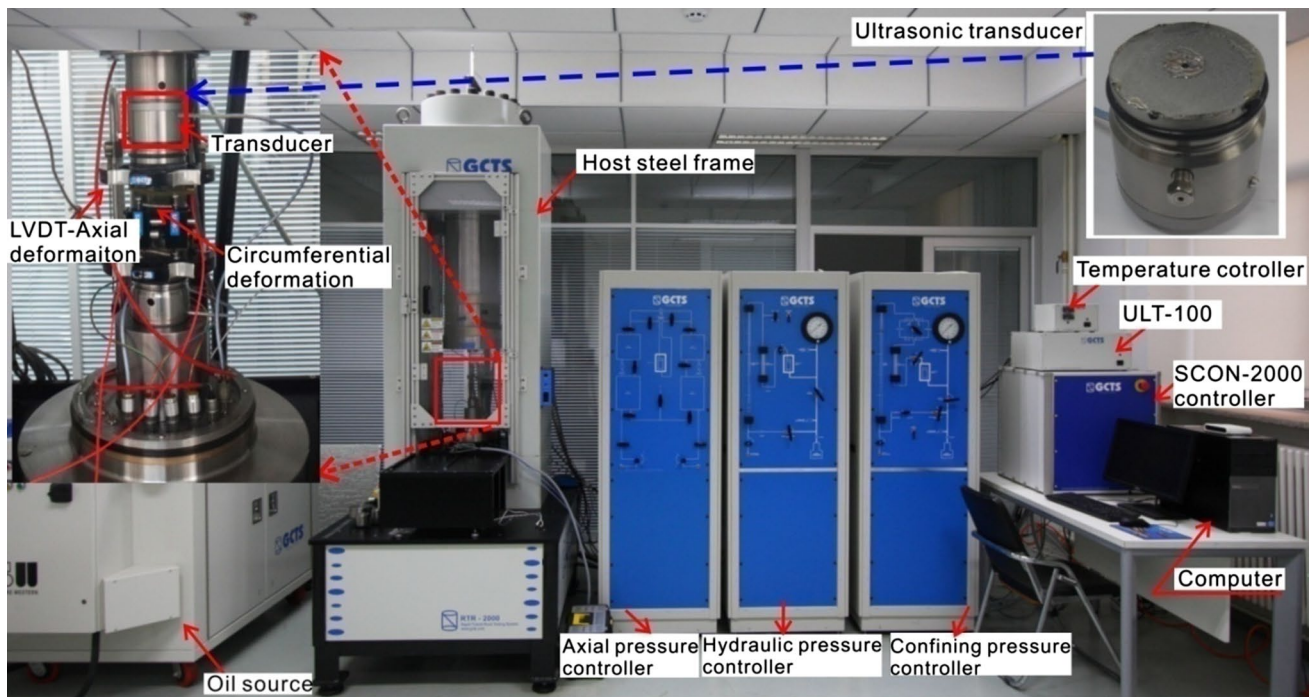


Fig. 3 GCTS RTR-2000 rock mechanics system used in the test

China. The shale cores, obtained from a depth about 20 m underground with alternating thin and thick layers, represent a carbonate-rich, mature gas shale. The average density of the shale samples is 2.62 g/cm^3 . For shale samples, cylindrical samples were in situ drilled out of the bulk material, under dry conditions with bedding plane inclinations of 0° , 15° , 30° , 45° , 60° , 75° , and 90° , which are defined as the intersection angle between the loading direction and the bedding face orientation. For the six kinds of rock samples,

they were prepared according to ISRM standards with a length-to-diameter ratio of approximately 2 (e.g., uniaxial compressive test is $100 \text{ mm} \times 50 \text{ mm}$ and tensile strength test is $50 \text{ mm} \times 25 \text{ mm}$) (ISRM 1981). The samples were ground to a planeness of 0.01 mm and the cylinder perpendicularity within 0.05 radians. The tolerance of planeness and cylinder perpendicularity of the tested samples met the standards of the ISRM-suggested method. Partial rocks used in the experiment are shown in Fig. 2.

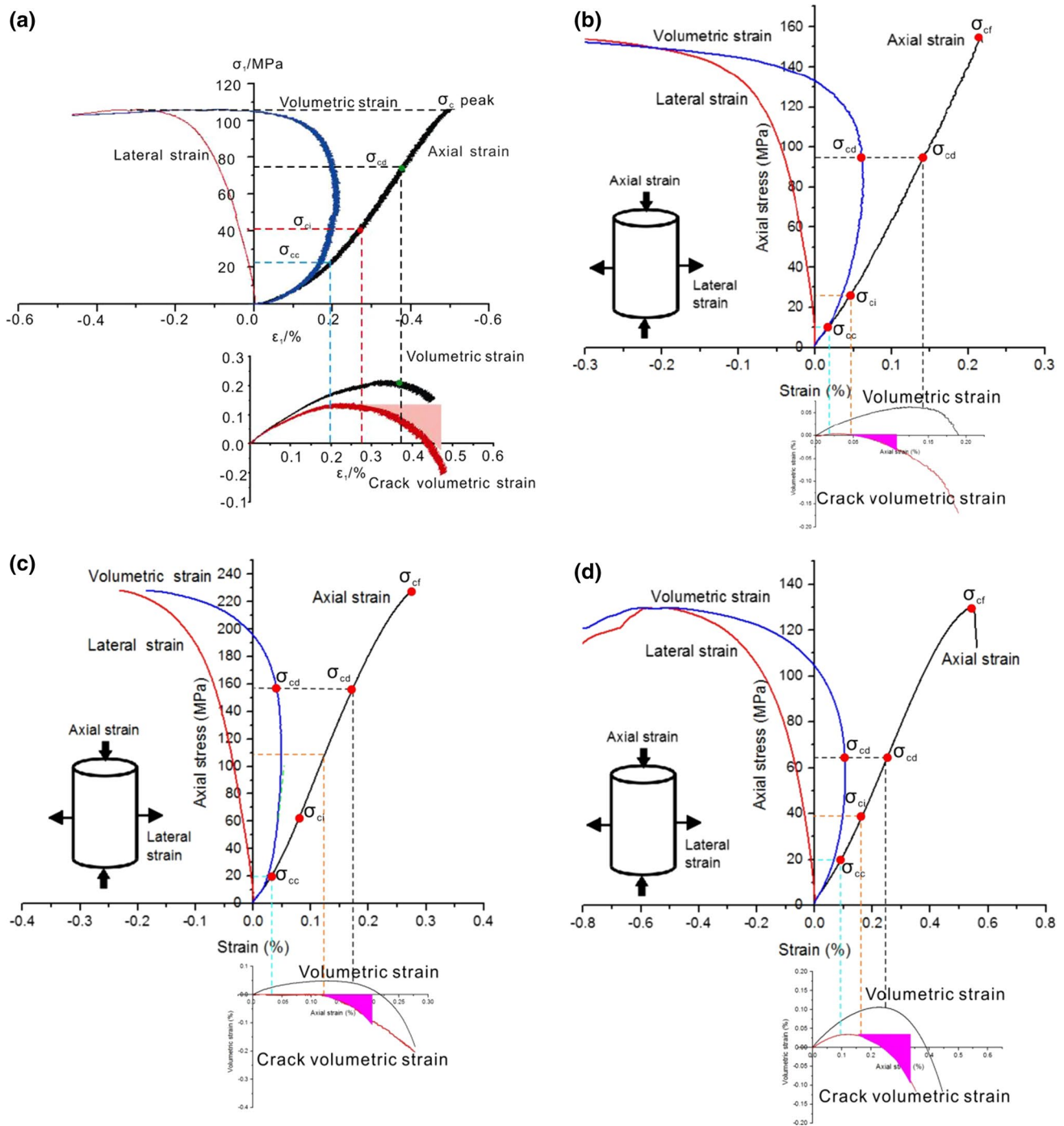


Fig. 4 Stress strain curves and crack initiation stress curves for typical samples. **a** Diorite sample #13; **b** granite sample #1; **c** marble sample #1; **d** sandstone sample #1; **e** shale sample with 0° orientation; **f** shale sample with 90° orientation

Experimental setup

The UCS tests were performed at a servo-controlled deformation apparatus (GCTS RTR-2000). The maximum applied axial force and frame stiffness are 4600 kN and 10.05 MN/mm, respectively. The apparatus can provide a maximum confining pressure of 210 MPa. The dynamic frequency of

the machine is 0–10 Hz. It can test the rock sample under the maximum temperature of 200° . A LVDT gauge was installed onto the sample to measure the axial strain and lateral strain. The axial loading was carried out under strain control with loading rate of 0.06 mm/min (strain rate of $1.0e^{-5} s^{-1}$) for UCS test. During the uniaxial compressive test, two strain gauges measuring the axial and lateral deformation were

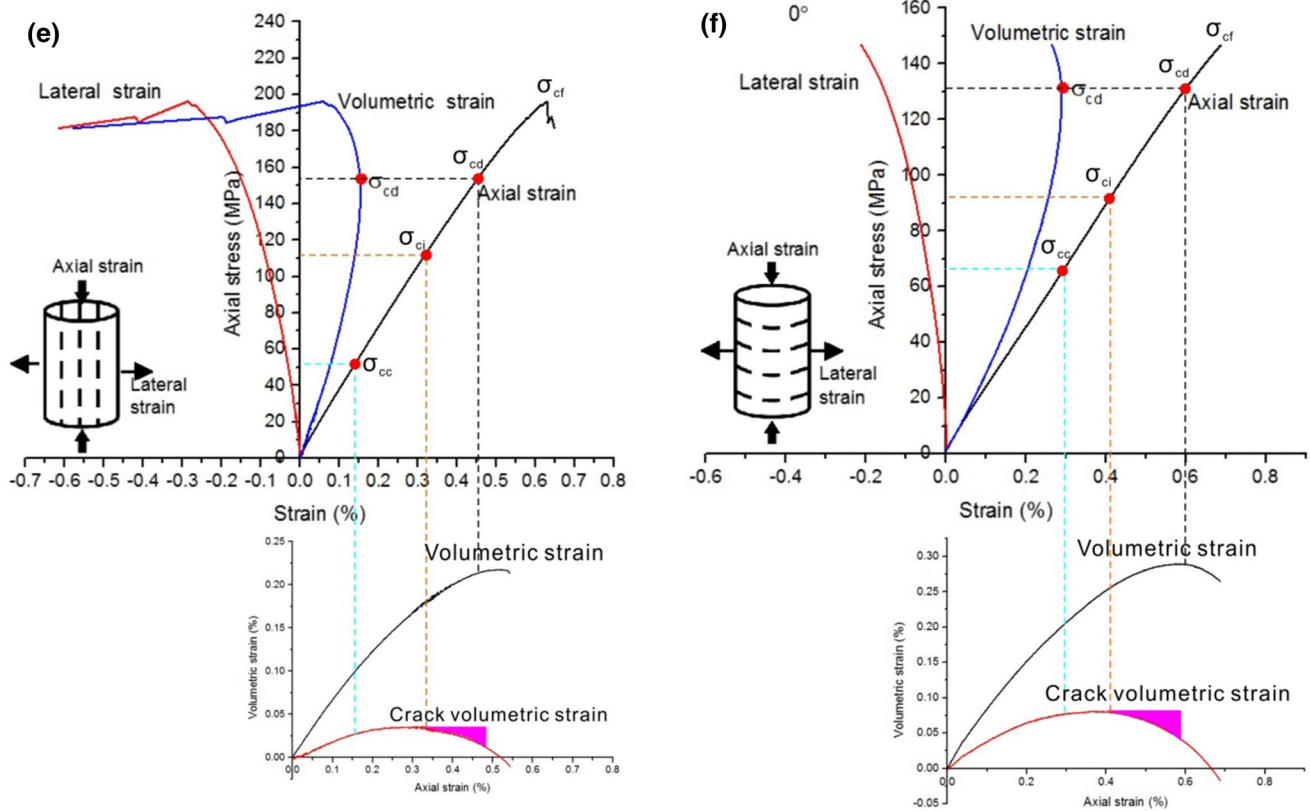


Fig. 4 (continued)

installed on rock samples, and the axial stress, axial strain, lateral strain, and circumferential strain can be recorded simultaneously at the same sampling frequency during the whole deformation process. The tensile strength of rock is determined by Brazilian tests, and the loading rate is 0.1 mm/min. The crack initiation stress is calculated using the method proposed by Martin and Chandler (1994): crack volumetric strain approach. Because the defined brittleness index in this work is strongly related to the rock mechanical parameters, therefore, among many of the definitions in Table 1, brittleness indexes B19, B20, B21, and B22 are used to calculate the brittleness. Based on the experimental results, we further discuss the relationships between B19, B20, B21, B22, and B23 (σ_{ci}/σ_c).

Calculation of σ_{ci} for typical samples

From the crack volumetric strain curves, the crack initiation stress is obtained for different rock samples. We plot the complete stress strain curve and crack volumetric strain curve for diorite, granite, marble, sandstone, and shale, as shown in Fig. 3. Due to the difference in mineral composition and microscopic structural fabric, the heterogeneity characteristics for these samples are different; therefore, the crack initiation stress level is different.

For these six samples, the value of crack initiation stress level is 0.55, 0.15, 0.48, 0.31, 0.60, and 0.64, respectively (Fig. 4).

Testing results and correlation analysis

Case 1: Medium- to coarse-grained diorite

According to the ISRM-suggested methods (ISRM 1981), the tested rock belongs to strong ($80 \text{ MPa} < \sigma_c < 100 \text{ MPa}$) and very strong ($\sigma_c > 100 \text{ MPa}$) rocks. The average compressive and tensile strength were 103 and 7.66 MPa, respectively. According to the analysis in “Methods” section, σ_{ci} is calculated by the crack volumetric strain curve. Uniaxial compression strength, Brazilian tensile strength values, and the crack initiation stress were viewed as first-hand data, and the brittleness index values of B19, B20, B21, and B22 were obtained using Eqs. (1)–(4), respectively (Table 1). Regression analysis was used to explore their relationship, and the equation with good correlations and the best-fit line was determined for each regression. Figure 5 shows the relationship between B19, B20, B21, B22, and B23 (σ_{ci}/σ_c). It is seen that there is no evident relation between the brittleness B21, B22, and B23 (i.e., there is a lower correlation coefficient of 0.627 and 0.621 that is found between them).

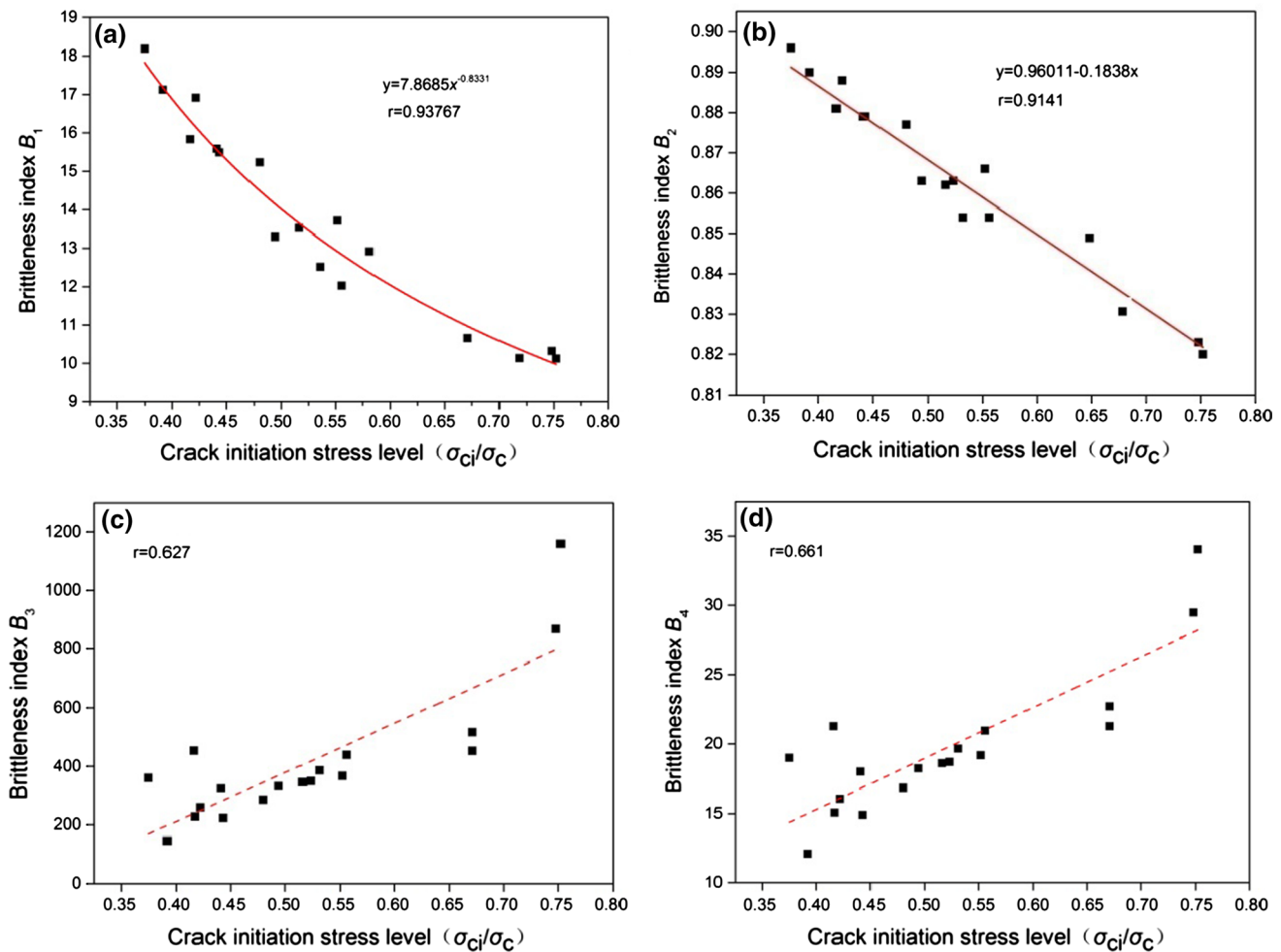


Fig. 5 Plots of the relationships between B19, B20, B21, B22, and B23 (σ_{ci}/σ_c) for coarse-grained diorite

However, there are significant relations between the brittleness values B19, B20, and σ_{ci}/σ_c . The correlation coefficients are 0.937 and 0.913, respectively. The relation follows a power function and linear function, respectively. As shown in Fig. 5, the brittleness decreased with increasing σ_{ci}/σ_c . The regression equations are as follows:

$$B19 = 7.8685(\sigma_{ci}/\sigma_c)^{-0.8333}, \quad R^2 = 0.937; \quad (8)$$

$$B20 = 0.96011 - 0.1838(\sigma_{ci}/\sigma_c), \quad R^2 = 0.913. \quad (9)$$

Case 2: Coarse-grained granite

The rock mechanical parameters were obtained as stated above; brittleness index of B19, B20, B21, and B22 is also calculated using the method mentioned above. UCS for the samples ranges from 99 to 160 MPa, tensile strength is between 3 and 6 MPa, and crack initiation stress level ranges from 0.15 to 0.31. We used regression analysis to study their relationship, and the equation of the correlation coefficients

and the best-fit line and were determined for each regression. Figure 6 shows the relationship between B19, B20, B21, B22, and B23 (σ_{ci}/σ_c). From the results, a strong correlation exists between B19, B20, and B23 (σ_{ci}/σ_c) and the correlation coefficients are 0.977 and 0.985, respectively. However, no evident relation exists between the brittleness B21, B22, and σ_{ci}/σ_c . The regression equations are:

$$B19 = 10.761(\sigma_{ci}/\sigma_c)^{-0.624}, \quad R^2 = 0.977; \quad (10)$$

$$B20 = -0.991 - 0.194(\sigma_{ci}/\sigma_c), \quad R^2 = 0.985. \quad (11)$$

Marble

Figure 7 shows the test results for the marble samples. UCS value ranges between 200 and 230 MPa. For tensile strength, the value ranges between 10 and 16 MPa. The crack initiation stress was calculated from the crack volumetric strain, and crack initiation stress level ranges

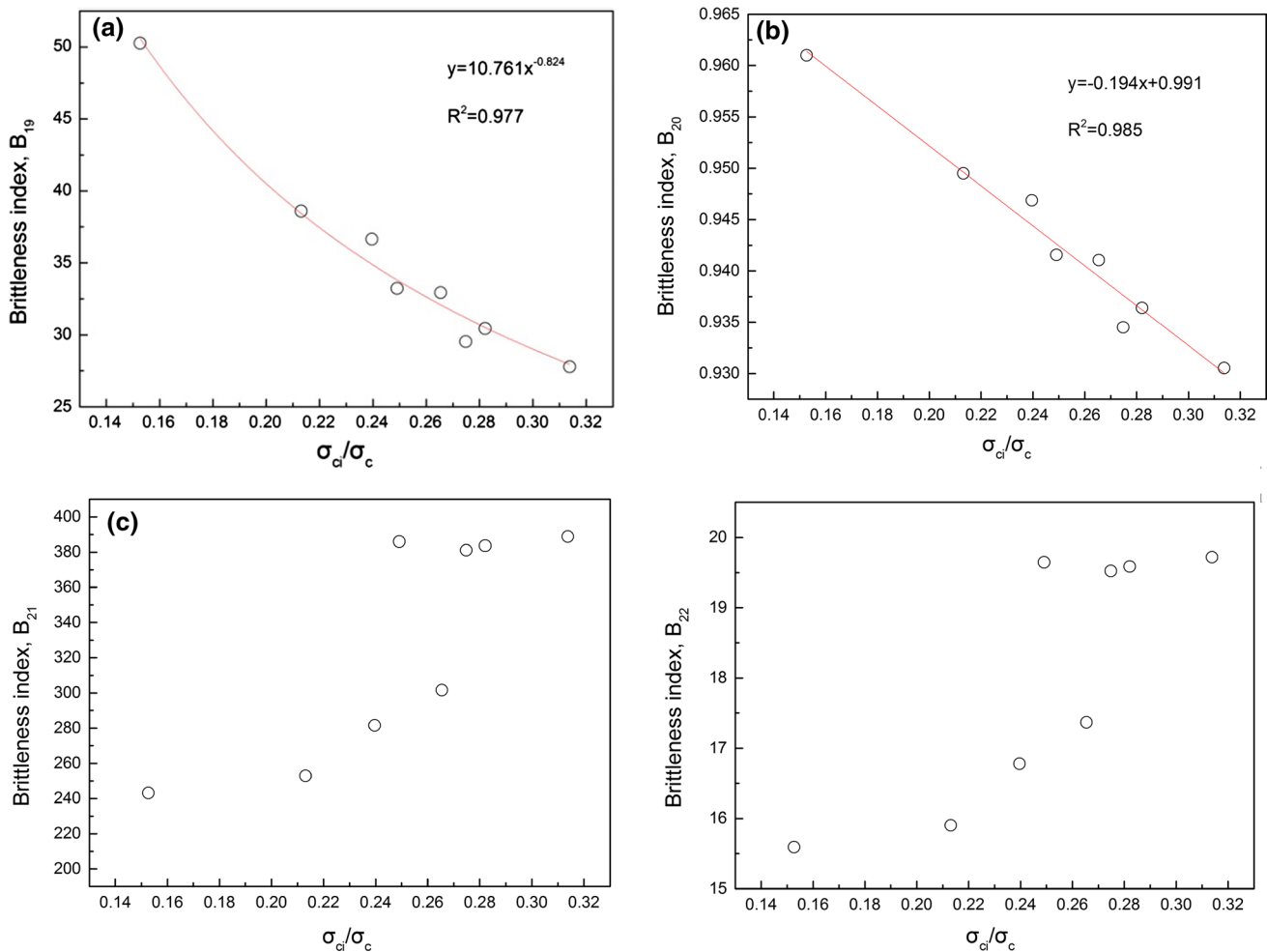


Fig. 6 Plots of the relationships between B19, B20, B21, B22, and B23 (σ_{ci}/σ_c) for granite

from 0.48 to 0.55, with an average value of 0.51. From the regression results for B20, B21, B22, and B23 (σ_{ci}/σ_c), an obvious correlation exists between B19, B20, and B23 (σ_{ci}/σ_c) and the correlation coefficients are 0.891 and 0.903, respectively. However, no evident relation between the brittleness B21, B22, and σ_{ci}/σ_c is found. The regression equations are as follows:

$$B19 = 2.625(\sigma_{ci}/\sigma_c)^{-2.987}, \quad R^2 = 0.891; \quad (12)$$

$$B20 = 1.187 - 0.585(\sigma_{ci}/\sigma_c), \quad R^2 = 0.903. \quad (13)$$

Case 4: Tight sandstone

Using the same method mentioned above, the basic rock mechanical parameters and the associated brittleness index are obtained. UCS of sandstone is between 90 and 131 MPa, tensile strength obtained by Brazilian test ranges between

3 and 6 MPa, and the crack initiation stress is between 0.3 and 0.5. Using regression analysis to obtain the relationship between B19, B20, B21, B22, and B23 (σ_{ci}/σ_c). Figure 8 plots the relationship between B20, B21, B22, and B23 (σ_{ci}/σ_c). From the results, there exists a strong correlation between B19, B20, and B23 (σ_{ci}/σ_c) and the correlation coefficients are 0.823 and 0.834, respectively. However, no evident relations are found between the brittleness B21, B22, and σ_{ci}/σ_c . The regression equations are as follows:

$$B19 = 8.347(\sigma_{ci}/\sigma_c)^{-2.987}, \quad R^2 = 0.823; \quad (14)$$

$$B20 = 0.999 - 0.223(\sigma_{ci}/\sigma_c), \quad R^2 = 0.845. \quad (15)$$

Case 5: Shale

The UCS of shale first decreases and then increases with the increase in orientation; the changes in UCS against orientation show a “U” shape. The UCS value ranges from 84 to 192 MPa, it is the maximum for a sample with 0°

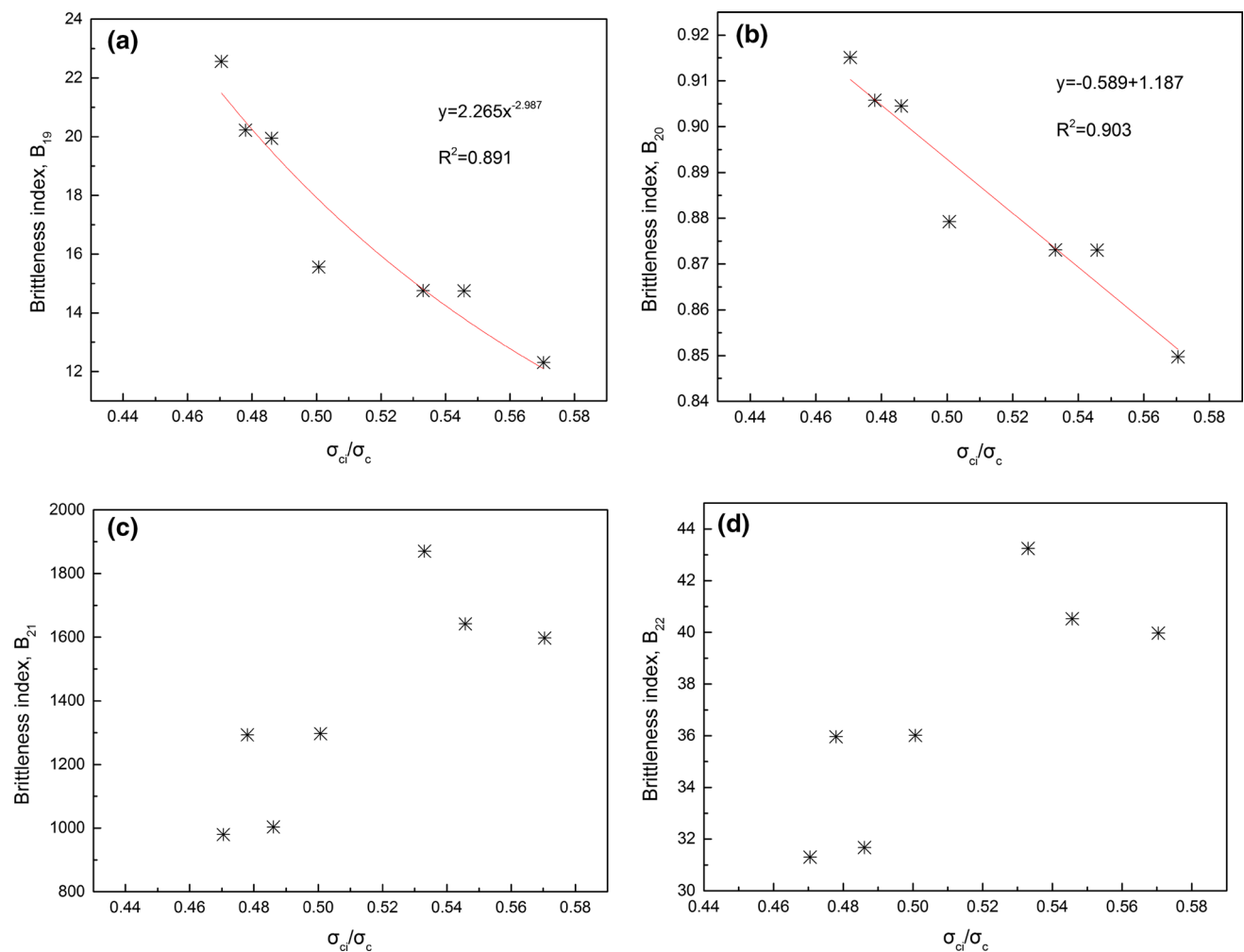


Fig. 7 Plots of the relationships between B_{19} , B_{20} , B_{21} , B_{22} , and B_{23} (σ_{ci}/σ_c) for marble

orientation, and it is the minimum for a sample with 30° inclination. For tensile strength, the value ranges between 4 and 10 MPa, it also shows an obvious anisotropy. The crack initiation stress was calculated from the crack volumetric strain, and typical curves for sample with 0° and 90° orientation are shown in Fig. 4. The value of B_{23} for shale samples with different orientation is different, and it shows strong anisotropic characteristics. For shale sample with 30° orientation, B_{23} is the maximum with its value of 0.62; however, for shale sample with 90° orientation, B_{23} is the minimum with its value of 0.56. Regression analysis is used to explore the relationship between them, and the equations which have best correlation coefficients were determined for each regression. Figure 9 shows the relationship between B_{19} , B_{20} , B_{21} , B_{22} , and B_{23} (σ_{ci}/σ_c). It can be seen that there is no evident relation between the brittleness B_{19} , B_{20} , and σ_{ci}/σ_c . However, obvious relationships exist between

the brittleness indexes B_{21} , B_{22} , and σ_{ci}/σ_c . The correlation coefficients are 0.711 and 0.711, respectively. The regression equations are as follows:

$$B_{21} = 7.300(\sigma_{ci}/\sigma_c)^{-1.863}, \quad R^2 = 0.711; \quad (16)$$

$$B_{22} = 0.999 - 0.223(\sigma_{ci}/\sigma_c), \quad R^2 = 0.711. \quad (17)$$

Discussion

From the experimental results, B_{23} as a new brittleness index to study the rock brittleness, the correlation between brittleness indexes (i.e., B_{19} , B_{20} , B_{21} , B_{22} , and B_{23}) defined based on σ_c , σ_{ci} , and σ_t is investigated. For the UCS test, those parameters are basic and important parameters to reflect the strength and deformation characteristics of brittle rock. Because of the difference in rock mineral composition

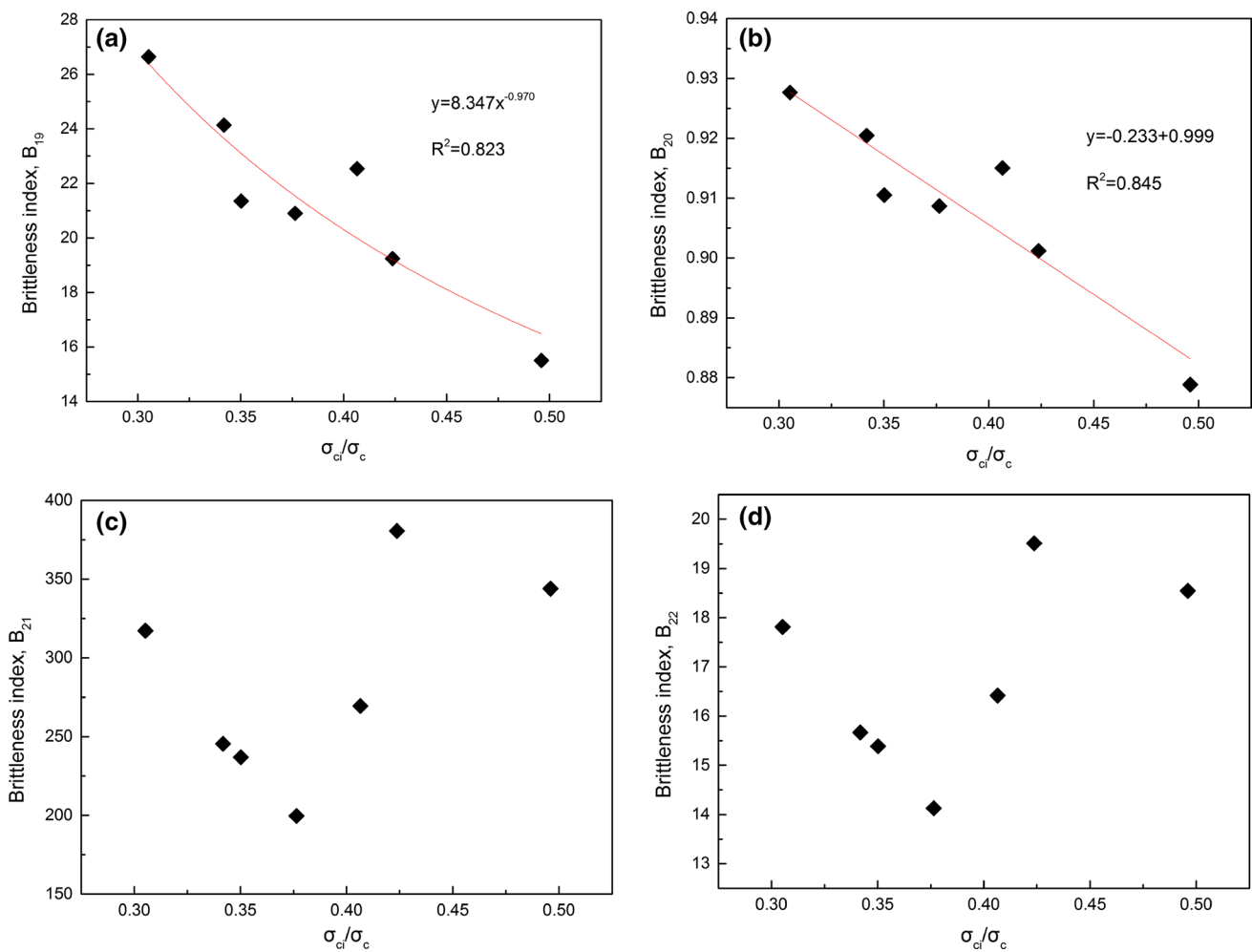


Fig. 8 Plots of the relationships between B19, B20, B21, B22, and B23 (σ_{ci}/σ_c) for tight sandstone

and microscopic fabric characteristics, crack initiation stress level ($B_{23} = \sigma_{ci}/\sigma_c$) presents obvious discrepancy. Experimental results show that the brittle index defined in this paper can well reflect the fabric inhomogeneity and structural heterogeneity. For the tested diorite, granite, sandstone, and marble, a correlation exists between B19, B20, and B23; however, for the anisotropic shale, an obvious correlation is found between B21, B22, and B23. These results indicate that index of B23 depends on the structural characteristics of rock. The tested shale samples are typical anisotropic material, and pronounced bedding plane develops during the diagenetic process. Due to the presence of foliation, bedding planes, cleavage, schistosity, and macro- or micro-natural fractures, the gas/oil shale is characterized by anisotropy. These structural characteristics result in the obvious anisotropy and heterogeneity characteristics, the existence of

bedding face alters not only its structural characteristics, but also its mechanical properties (e.g., modulus, fracture toughness, failure modes, stress–strain behaviors, and brittleness). Compared to other relative homogenous rocks in this study, correlation among the brittleness indexes is different for shale samples (Fig. 10).

The absence of universally accepted definition and measurement of brittleness has led to various methods or models for its quantification, as already summarized in Table 1. Generally, it has been long accepted that formations with high brittleness are easy to be fractured, but this assumption is not always true. Taking dolomitic limestone for example, fracture barrier occurs in this high brittleness rock, because fracture gradient in dolomitic limestone formation is higher than in shale formation, and the fracture is different to cross it (Jin et al. 2014). Therefore, it may not be reasonable for

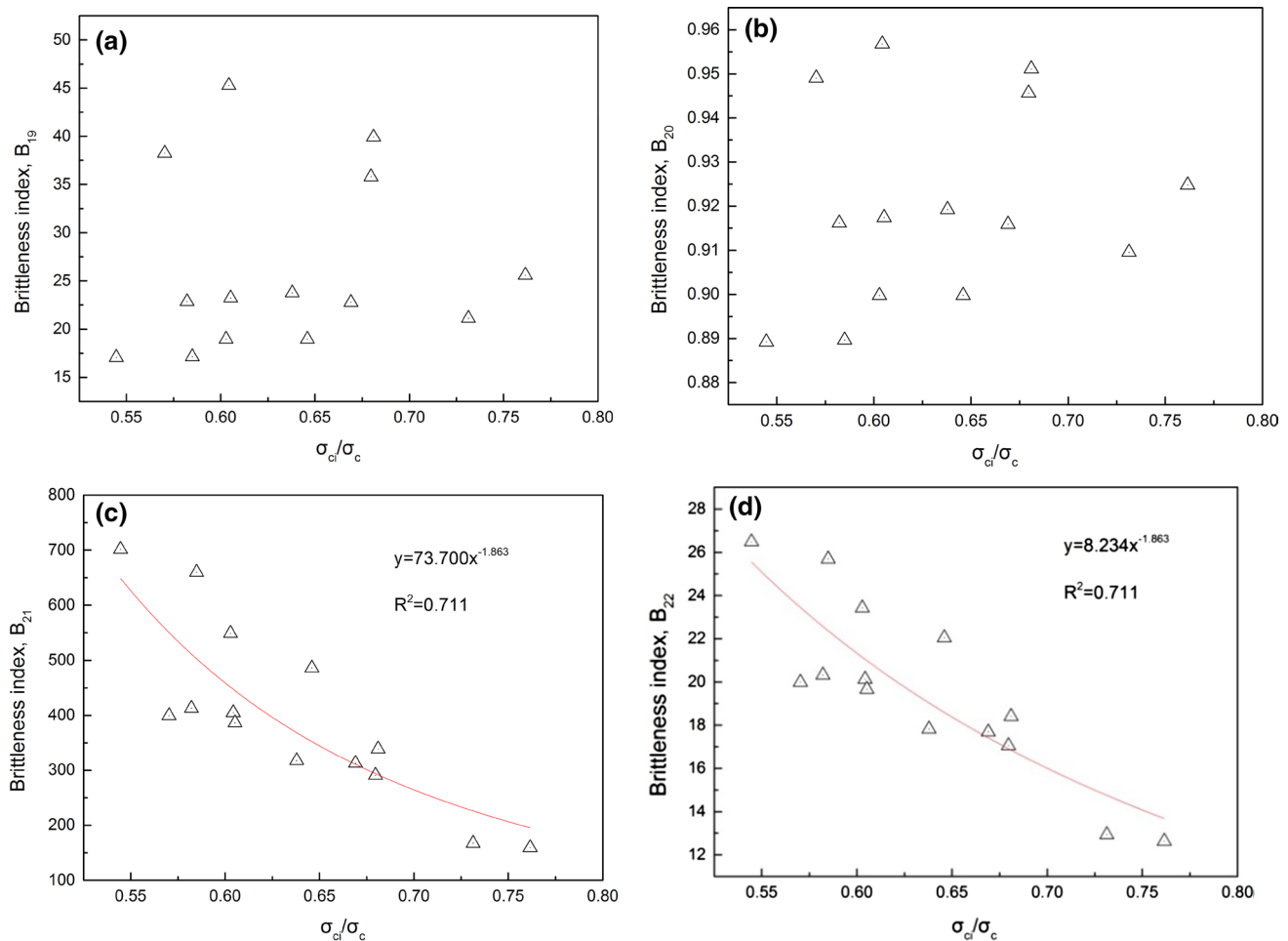


Fig. 9 Plots of the relationships between B_{19} , B_{20} , B_{21} , B_{22} , and B_{23} (σ_{ci}/σ_c) for the anisotropic shale

formations to be easily fractured with high brittleness and brittleness index based on rock geomechanics should reflect the fracture pattern and crack density; in other works, we should establish relationship between the brittleness index and fracturing effectiveness. Here, the proposed brittle index of B_{23} , objectively, can better reflect the fracturing characteristics and the associated fracture pattern after experiment. For granite, marble, and sandstone, the average B_{23} value is 0.242, 0.387, and 0.512, respectively. Figure 11 shows the failure morphology of these three kinds of rock. It can be seen that the fracture scale is the largest for rock with a lower B_{23} value.

From the fracture pattern observation on sample surface alone one may not verify the reliability that B_{23} can reflect the fracturing effectiveness or the fracability of rock formations. We further study the fracture morphology in shale

sample using high-energy X-ray CT. Figure 11 plots typical CT images, and the cracks are identified for shale with orientations of 0° , 15° , 30° , 45° , 60° , 75° , and 90° , respectively. From the observation of the CT images, the fracture scale is the maximum for sample with 90° orientation; however, it is the minimum for sample with 30° orientation. We plot the relationship between fracture density (which is defined as the ratio of total crack area to the sample section) and orientation, as shown in Fig. 11. Quantitative analysis also indicates that fracture density is larger for shale samples with 90° orientation. The relationship between the fracture density and the B_{23} is shown in Fig. 13, it shows that a good correlation exists between them, and the sample with larger stimulated fracture area corresponds to a lower σ_{ci}/σ_c value (Fig. 12).

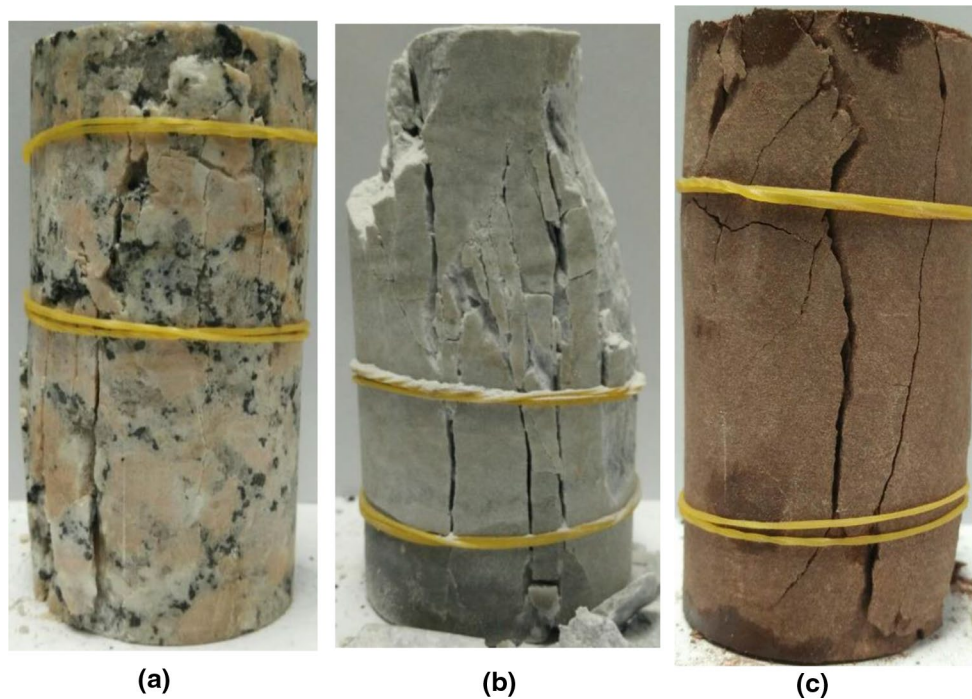


Fig. 10 Failure morphology of typical rock samples for granite, marble, and sandstone. **a** Granite; $B_{23} = 0.242$. **b** Marble; $B_{23} = 0.387$. **c** Sandstone; $B_{23} = 0.511$

Conclusions

Brittleness is known as one of the most important properties of rock material. Brittleness of rock is very closely related to the stability of the rock mass engineering and reservoir engineering. Therefore, it is significant and important to conduct some related research on rock brittleness. In this work, we have conducted plenty of UCS tests for diorite, granite, marble, sandstone, and shale and a new brittleness index defined as σ_{ci}/σ_c is used to evaluate the brittleness and fracture pattern. The link between brittleness and σ_{ci}/σ_c was explored from the theoretical and experimental analysis. The relations between the brittleness and σ_{ci}/σ_c were statistically investigated using the raw data obtained from experimental data of the five examples. Some main conclusions are drawn as follows:

1. Brittleness index of B_{23} reflects the rock anisotropy and non-homogeneity, and it is strongly related to the rock mesoscopic fabric. A strong relationship between the brittleness indexes B_{19} , B_{20} , B_{21} , B_{22} , and B_{23} (σ_{ci}/σ_c) was found. Due to the differences in rock fabric, the regression results are various for different rocks. It can be concluded that index of σ_{ci}/σ_c can be viewed as a promising index for the evaluation of rock brittleness.
2. For the studied rocks, a negative correlation exists between B_{19} , B_{20} , B_{21} , B_{22} , and B_{23} . The results indicate that crack initiation stress level decreases with the increase in brittleness and micro-fracture would occur earlier during deformation. For sample with low σ_{ci}/σ_c value, larger fracture network density may be stimulated.
3. Fracture morphology description and CT images analysis indicate that rock brittleness has certain internal rela-

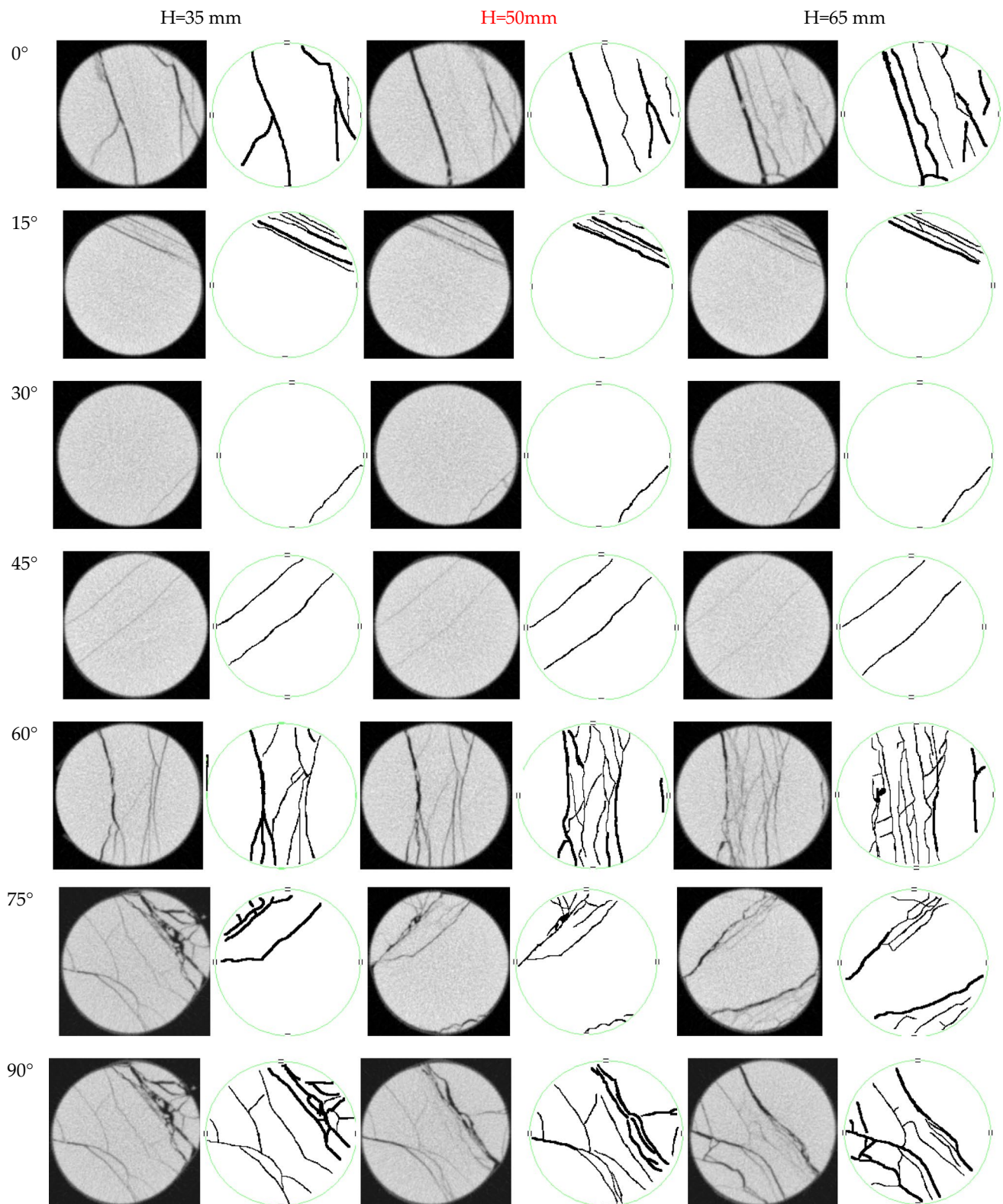


Fig. 11 Crack morphology visualized by CT imaging. Image 2D reconstructions of shale samples with different inclination, CT scans at different positions, at 35, 50, and 65 mm, from the top of the samples

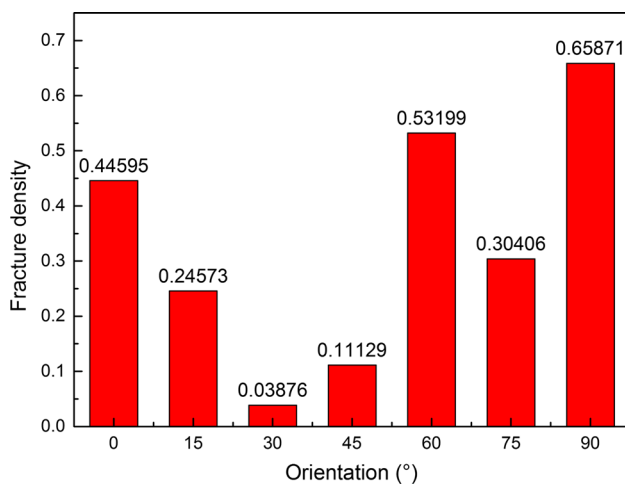


Fig. 12 Plot of fracture density against bedding plane orientation

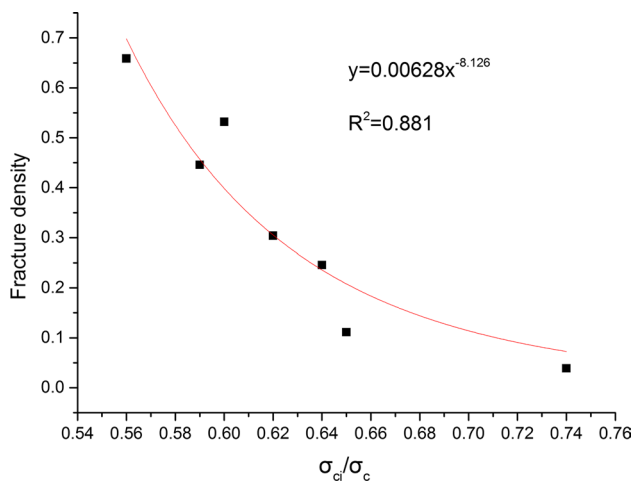


Fig. 13 Plot of fracture density against crack initiation stress level (B23)

relationship with crack initiation stress level. For shale samples studied in this work, a good correlation has been found between the fracture density and σ_{ci}/σ_c , which is in good agreement with the CT scanning results.

Acknowledgements The authors would like to thank the editors and the anonymous reviewers for their helpful and constructive comments. This work was supported by the Beijing National Science Foundation of China (Grants No. 8164070), National Natural Science Foundation of China (Grants No. 41502294), and Fundamental Research Funds for the Central Universities.

Authors' contribution Yu Wang and C. H. Li designed the theoretical framework; Yu Wang conducted the experiment, analyzed the experimental data, and wrote the manuscript; Y. Z. Hu, T. Q. Mao, and B. Zheng corrected the figures.

Compliance with ethical standards

Conflict of interest The authors declare no conflict of interest.

References

- Altindag R (2002) The evaluation of rock brittleness concept on rotary blast hole drills. *J S Afr Inst Min Metall* 102(1):61–66
- Altindag R, Guney A (2010) Predicting the relationships between brittleness and mechanical properties (UCS, TS and SH) of rocks. *Sci Res Essays* 16:2107–2118
- Andreev GE (1995) *Brittle failure of rock materials*. CRC Press, Boca Raton
- Aubertin R (2010) Assessment of some brittleness indexes in rock-drilling efficiency. *Rock Mech Rock Eng* 43:361–370
- Bieniawski ZT (1967) Mechanism of brittle fracture of rock, part I—theory of the fracture process. *Int J Rock Mech Min Sci Geomech Abstr* 4:395–406
- Bishop AW (1967) Progressive failure—with special reference to the mechanism causing it. Paper presented at geotechnical conference, Oslo, Norway
- Blindheim OT, Bruland A (1998) Boreability testing[C]//Norwegian TBM tunneling—30 years of experience with TBMs in Norwegian tunneling. Norwegian Soil and Rock Engineering Association, Trondheim, pp 29–34
- Bazant ZP, Kazemi MT (1990) Determination of fracture energy, process zone length and brittleness number from size effect, with application to rock and concrete. *Int J Fracture* 44:111–131
- Brace WF, Paulding B, Scholz C (1966) Dilatancy in the fracture of crystalline rocks. *J Geophys Res* 71:3939–3953
- Bruner KR, Smosna R (2011) A comparative study of the Mississippian Barnett Shale, Fort Worth Basin, and Devonian Marcellus Shale, Appalachian Basin. National Energy Technology Laboratory Rep., DOE/NETL-2011/1478
- Cai M (2010) Practical estimates of tensile strength and Hoek-Brown strength mi of brittle rocks. *Rock Mech Rock Eng* 43:167–184
- Cai M, Kaiser PK, Tasakab Y (2004) Generalized crack initiation and crack damage stress thresholds of brittle rock masses near underground excavations. *Int J Rock Mech Min Sci* 41:833–847
- Chen J, Zhang G, Chen H, Yin X (2014) The construction of shale rock physics effective emodel and prediction of rock brittleness. In: Proceedings of the 2014 SEG annual meeting, society of exploration geophysicists, pp 2861–2865
- Chong KK, Grieser W, Passman A, Tamayo H, Modeland N, Burke B (2010) A completions guide book to shale-play development: a review of successful approaches toward shale-play stimulation in the last two decades. Paper presented at Canadian Unconventional Resources and International Petroleum Conference, Calgary, Alberta, Canada, 19–21 Oct 2010
- Copur H, Bilgin N, Tuncdemir H (2003) A set of indices based on indentation test for assessment of rock cutting performance and rock properties. *J S Afr Inst Min Metall* 103(9):589–600
- Diederichs MS, Kaiser PK, Eberhardt E (2004) Damage initiation and propagation in hard rock during tunnelling and the influence of near-face stress rotation. *Int J Rock Mech Min Sci* 5:785–812
- Feng T, Xie XB (2000) Brittleness of rocks brittleness indexes for describing rock burst proneness. *Min Metall Eng* 20:18–20
- Gunaydin O, Kahraman S, Fener M (2004) Sawability prediction of carbonate rocks from brittleness indexes. *J S Afr Inst Min Metall* 104:1–6
- Guo Z, Chapman M, Li X (2012) Exploring the effect of fractures and micro-structure on brittleness index in the Barnett Shale. In: SEG annual meeting, Las Vegas, NV, pp 4609–4613

- Hajiabdolmajida V, Kaise PK, Martin CD (2003) Modelling brittle failure of rock. *Int J Rock Mech Min Sci* 39:731–741
- Honda H, Sanada Y (1956) Hardness of coal. *Fuel* 35:451–461
- Hucka V, Das B (1974) Brittleness determination of rocks by different methods. *Int J Rock Mech Min Sci Geomech Abstr* 11:389–392
- ISRM (1981) Rock characterization testing and monitoring. In: Brown ET (ed) ISRM suggested methods. Pergamon Press, Oxford
- Jarvie DM, Hill RJ, Ruble TE, Pollastro RM (2007a) Unconventional shale-gas systems: the Mississippian Barnett Shale of north-central Texas as one model for thermogenic shale-gas assessment. *AAPG Bull* 91:475–499
- Jarvie DM, Hill RJ, Ruble TE, Pollastro RM (2007b) Unconventional shale-gas systems: the Mississippian Barnett Shale of north-central Texas as one model for thermogenic shale-gas assessment. *AAPG Bull* 91(4):475–499
- Jin X, Shah SN, Roegiers JC (2014a) Fracability evaluation in shale reservoirs—an integrated petrophysics and geomechanics approach[C]//SPE hydraulic fracturing technology conference. Society of Petroleum Engineers, London
- Jin X, Shah SN, Truax JA (2014b) A practical petrophysical approach for brittleness prediction from porosity and sonic logging in shale reservoirs[C]//SPE annual technical conference and exhibition. Society of Petroleum Engineers, London
- Lawn BR, Marshall DB (1979) Hardness, toughness and brittleness: an indentation analysis. *J Am Ceram Soc* 62(7/8):347–350
- Li QG, Chen M, Jin Y (2012) Rock mechanics properties and brittleness evaluation of shale gas reservoir. *Pet Drill Tech* 40:18–22
- Luan X, Di B, Wei J, Li X, Qian K, Xie J, Ding P (2014) Laboratory measurements of brittleness anisotropy in synthetic shale with different cementation. In: Proceedings of the 2014 SEG annual meeting. Denver, Society of exploration geophysicists, pp 3005–3009
- Martin CD, Chandler NA (1994) The progressive fracture of Lac du Bonnet granite. *Int J Rock Mech Min Sci Geomech Abstr* 6:643–659
- Munoz H, Taheri A, Chanda EK (2016a) Fracture energy-based brittleness index development and brittleness quantification by pre-peak strength parameters in rock uniaxial compression. *Rock Mech Rock Eng* 49(12):4587–4606
- Munoz H, Taheri A, Chanda EK (2016b) Rock drilling performance evaluation by an energy dissipation based rock brittleness index. *Rock Mech Rock Eng* 49(8):3343–3355
- Nicksiar M, Martin CD (2012) Evaluation of methods for determining crack initiation in compression tests on low-porosity rocks. *Rock Mech Rock Eng* 45:607–617
- Nygård RM, Gutierrez M, Bratli RK, Høeg K (2006) Brittle–ductile transition, shear failure and leakage in shales and mudrocks. *Mar Pet Geol* 23(2):201–212
- Protodyakonov MM (1963) Mechanical properties and drillability of rocks[C]. In: Proceedings of the 5th symposium on rock mechanics. University of Minnesota Press, Twin Cities, USA, pp 103–118
- Quinn JB, Quinn GD (1997) Indentation brittleness of ceramics: a fresh approach. *J Mater Sci* 32(16):4331–4346
- Rickman R, Mullen M, Petre J, Grieser W, Kundert D (2008) A practical use of shale petrophysics for stimulation design optimization: all shale plays are not clones of the Barnett shale, paper presented at SPE In: Annual technical conference and exhibition, Denver, Colorado, USA, September 21–24, 2008
- Sih GC (1974) Strain–energy–density factor applied to mixed mode crack problems. *Int J Fract* 3: 305–321
- Sehgal J, Nakao Y, Takahashi H, Ito S (1995) Brittleness of glasses by indentation. *J Mater Sci Lett* 14(3):167–169
- Sun SZ, Wang KN, Yang P, Li XG, Sun JX, Liu BH, Jin K (2013) Integrated prediction of shale oil reservoir using pre-stack algorithms for brittleness and fracture detection. In: International petroleum technology conference, Beijing
- Tarasov BG (2001) New experimental physics and rock mechanics. United States, p 344
- Tarasov B, Potvin Y (2013) Universal criteria for rock brittleness estimation under triaxial compression. *Int J Rock Mech Min Sci* 59:57–69
- Vahid H, Peter K (2003) Brittleness of rock and stability assessment in hard rock tunneling. *Tunn Undergr Space Technol* 18(1):35–48
- Wang FP, Gale JF (2009) Screening criteria for shale-gas systems. *Geol Soc Trans Gulf Coast Assoc Geol Trans* 59:779–793
- Wang Y, Li X, Wu YF, Ben YX, Li SD, He JM, Zhang B (2014) Research on relationship between crack initiation stress level and brittleness indices for brittle rocks. *Chin J Rock Mech Eng* 33:264–275
- Wang DB, Ge HK, Wang XQ, Wang JB, Meng FB, Suo Y, Han P (2015) A novel experimental approach for fracability evaluation in tight-gas reservoirs. *J Nat Gas Sci Eng* 23:239–249
- Wang M, Li P, Wu X et al (2016) A study on the brittleness and progressive failure process of anisotropic shale. *Environ Earth Sci* 75(10):886
- Xia YJ, Li LC, Tang CA et al (2017) A new method to evaluate rock mass brittleness based on stress–strain curves of class I. *Rock Mech Rock Eng* 50(5):1123–1139
- Yagiz S (2002) Development of rock fracture and brittleness indices to quantify the effects of rock mass features and toughness in the CSM Model basic penetration for hard rock tunneling machines (Doctoral dissertation, Colorado School of Mines. Arthur Lakes Library)
- Yagiz S, Gokceoglu C (2010) Application of fuzzy inference system and nonlinear regression models for predicting rock brittleness. *Expert Syst Appl* 5:2265–2272
- Yarali O, Kahraman S (2011) The drillability assessment of rocks using the different brittleness values. *Tunn Undergr Space Tech* 26:406–414
- Zhang D, Ranjith PG, Perera MSA (2016) The brittleness indices used in rock mechanics and their application in shale hydraulic fracturing: a review. *J Petrol Sci Eng* 143:158–170
- Zhang X, Lu Y, Tang J, Zhou Z, Liao Y (2017) Experimental study on fracture initiation and propagation in shale using supercritical carbon dioxide fracturing. *Fuel* 190:370–378